Journal of Nuclear Materials 182 (1991) 52–59
North-Holland

Transgranular fracture of Fast Reactor irradiated stainless steel

I.J. Ford

Theoretical Studies Department, Materials and Manufacturing Technology Division, AEA Industrial Technology, Harwell Laboratory, Didcot, Oxon OX11 0RA, United Kingdom

Received 27 September 1990; accepted 6 October 1990

An understanding of the fracture of Fast Reactor fuel pin cladding can provide a basis for predicting the failure of fuel pins in normal reactor operation, or in assessing the severity of hypothetical accidents. Mechanistic modelling of the various failure modes is the most promising means of gaining such an understanding and we present here theories describing the transgranular mechanical fracture mode of 20% cold-worked AISI 316 steel. This is characterised by plastic yield deformation when the stress exceeds a yield stress. The main part of the development deals with the evolution of the yield stress under irradiation at high temperature. We also consider the evolution of the constitutive relations, especially the effect of cladding porosity on the ductility, and find that neutron-induced void swelling may be responsible for low failure strains in some circumstances.

1. Introduction

Cladding materials for Fast Reactor fuel pins need to be carefully chosen if they are not to fracture under the hostile conditions to be found within a reactor core. The high temperatures and fast neutron irradiation flux together with stresses arising from contact with the fuel pellet, or from internal fission gas pressurisation, give rise to creep deformation and neutron-induced void swelling. In addition, the yield behaviour of the cladding material is altered, largely to the detriment of its endurance. A mechanistic model of yield plasticity is presented here which attempts to understand plastic yield deformation of irradiated cladding, and from which a theory of transgranular cladding fracture can be developed. The model is intended for use in fuel pin modelling codes such as TRAFIC [1] and TRANSURANUS [2], which are based largely on a mechanistic understanding of fuel pin behaviour.

The need to develop mechanistically based models of failure processes is underlined by the lack of precision found when various empirical rules are applied. Our view is that this is because such rules fail to identify individual mechanisms of fracture. The transgranular mode discussed here operates at low temperatures and high stresses and usually induces a fast failure. The phenomenology of transgranular failure has traditionally been founded on the concept of instantaneous plastic yield deformation when the applied stress exceeds a critical value known as the yield stress. Fracture occurs when the stress exceeds an ultimate tensile stress, or equivalently, when the yield strain reaches a failure ductility. These criteria underline the importance of the constitutive relation for the yield process. Our approach has followed this phenomenology, but has attempted to model both the yield stress and the constitutive relation from a viewpoint of dislocation theory. The complexity of the engineering materials considered for reactor applications, however, makes any first principles approach oversimplified, and we use experimental data to fix the parameters of the models.

The evolution of the yield stress is discussed in the next section, where we consider the influence of recovery and recrystallisation at high temperatures, and irradiation damage due to the fast neutron flux. This leads on to a consideration of the yield constitutive relation in section 3. In section 4 we address the criterion for fracture during yield, the onset of instability. We note that cladding porosity can affect yield in two ways: the reduction of the yield stress due to stress concentration by the pores, and the lessening of work hardening due to pore expansion. Both these effects may be induced by the presence of neutron-induced voids in the cladding, and we demonstrate a correlation between high volume swellings and low ductilities. We summarise our conclusions in section 5.

Elsevier Science Publishers B.V. (North-Holland)

2. The yield stress

Plastic deformation corresponds to a flow of dislocations through the material. Barriers opposing this motion may be overcome athermally, by applying a sufficient driving force to overcome resistance, or thermally, where energy fluctuations allow barrier penetration with a certain probability. These two mechanisms correspond in general terms to the time-independent yield and time-dependent creep modes of plasticity. There can be a number of types of barriers to dislocation motion in real materials. Any inhomogeneity in the crystal lattice will impede the glide of dislocations, and this can include point defects, voids or precipitates, grain boundaries, or other dislocations. The effect of a static homogeneous dislocation density ρ can be considered as a representative example. The barrier forces have complex spatial variations in such an arrangement. The opposing stress on a mobile dislocation due to a dislocation network is proportional to $\rho^{1/2}$ [3], corresponding to an inverse dependence of the opposing force upon the distance to the nearest inhomogeneity. A starting point for modelling the yield stress σ_y is therefore the expression:

$$\sigma_y = \sigma_0 + A\alpha^{1/2}, \tag{1}$$

where σ_0 is the yield stress of annealed material and A is a ρ-independent function. The hardness parameter α is proportional to the dislocation density. Later on we shall describe the evolution of α corresponding to changes in ρ. Initially ρ is proportional to the cold work strain ϵ_{cw}, and the proportionality factor between ρ and α is chosen such that $\alpha = \epsilon_{cw}$ before irradiation.

A first development of this simple picture is to take into account the temperature dependence of σ_y through the parameters σ_0 and A. For this, we use experimental data corresponding to tensile tests on unirradiated cladding, at temperatures reached at rapid heating rates such that recovery (the removal of dislocations) does not operate, i.e. ρ is constant.

The material we shall model is 20% cold-worked AISI 316 stainless steel, which has been a reference cladding material for Fast Reactors. The data shown in fig. 1 produce the following fits in MPa, with the temperature T in °C:

$$\sigma_0 = 162 - 0.0721T \quad [4],$$

$$A = 1091.2 - 0.286T \quad \text{for } T < 500\,^\circ\text{C},$$
$$= 1650.2 - 1.404T \quad \text{for } 500\,^\circ\text{C} < T < 538\,^\circ\text{C},$$
$$= 1650.2 - 1.404T - 0.08(T - 538)\ln(50/\dot{\epsilon}) \quad \text{for } T > 538\,^\circ\text{C} \quad [5,6].$$

These empirical fits can be interpreted in the following way. Below 500 °C the dislocations overcome barriers to their motion athermally, and in models A would be proportional to the shear modulus of the material, with a weak temperature dependence. In the high temperature regime, however, thermal penetration of the barriers comes to dominate. The two mechanisms can be considered to act in parallel. A simple model of thermally-induced obstacle penetration yields the following form:

$$\sigma_y = \frac{1}{v_a}[U_0 - kT \ln \dot{\epsilon}_0/\dot{\epsilon}], \tag{2}$$

where v_a is the activation volume (proportional to $\rho^{-1/2}$), U_0 is the energy required to overcome the barrier athermally, and $\dot{\epsilon}_0$ is a reference deformation rate. The yield stress has a reasonably low sensitivity to the applied deformation rate ($\dot{\epsilon} \gg \dot{\epsilon}_0$) but a stronger temperature dependence than in the low temperature region.

This changeover in mechanism may be linked with the evolution of the dislocation structure from a uniform tangle, at low temperatures, to a sub-grain cellular arrangement at higher temperatures [7] where the nature of the obstacles tends to involve short-range forces, which can be overcome by thermal fluctuation.

Eq. (1) is the basis of subsequent development which allows for the evolution of σ_y at high temperature and under irradiation. The dislocation density, whether in a uniform or cellular arrangement, will tend to anneal out as a result of the high temperature-enabled climb-to-

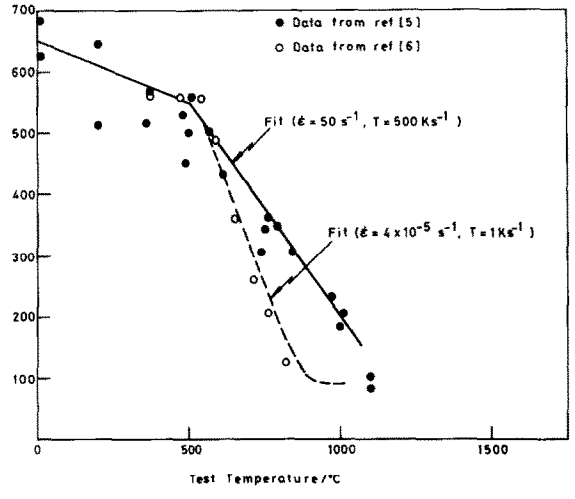

Fig. 1. Temperature dependence of yield stress of unirradiated 20% cold-worked AISI 316 steel including effects of heating rate and deformation rate.

gether of pairs of dislocations of opposite Burger's vectors [8]. The rate of thermal recovery will be determined by D_s, the vacancy self-diffusion coefficient of the material, and will be quadratic in ρ. As for the effect of irradiation, we assume that dislocations are generated at a rate proportional to the displacement damage rate $\dot{D}$ (in dpa (NRT Fe)/s) but that the network introduced will saturate at a particular level corresponding to the setting up of a dynamic equilibrium between dislocation generation and irradiation-enabled climb to mutual annihilation. The removal rate will again be quadratic in ρ [9], but now proportional to $\dot{D}$. These effects are all represented in the following equation for $\dot{\alpha}$:

$$\dot{\alpha} = a\dot{D} - (\alpha - \alpha_0)^2(bD_s + c\dot{D}), \tag{3}$$

which contains three parameters a, b and c which may be considered temperature and dose rate independent. The hardness α_0 describes a limiting dislocation density which is stable against climb. A non-zero α_0 sets a limit on the extent to which α can be reduced by high temperature recovery. There is, however, a second process reducing the material to the annealed state, namely recrystallisation. This corresponds to the movement of grain boundaries, creating perfect crystal lattice, free of dislocations. To allow for this we replace eq. (1) by

$$\sigma_y = \sigma_0 + A((1 - f_R)\alpha)^{1/2}, \tag{4}$$

where f_R is the volumetric fraction of recrystallised material. The evolution of f_R is described by a simple grain growth model [10]:

$$\dot{f}_R = K_R f_R (1 - f_R) \exp(-T_G/T), \tag{5}$$

which describes an initially slow rate of recrystallisation, becoming much more rapid after an incubation period which is very temperature dependent, being proportional to the exponential factor. The recrystallisation annealing operates at generally higher temperatures than climb recovery, and can produce a much more softened material.

The six parameters in the yield stress evolution model can be set by reference to different sets of experimental data which demonstrate the various individual phenomena which we are trying to represent. The high temperature annealing data [11] in fig. 2 illustrate recovery and recrystallisation and can be fitted with $K_R = 4.82 \times 10^{19}$ s^{-1}, $T_G = 61000$ K and $b = 1.2 \times 10^{17}$ m^{-2}, with $D_s =$

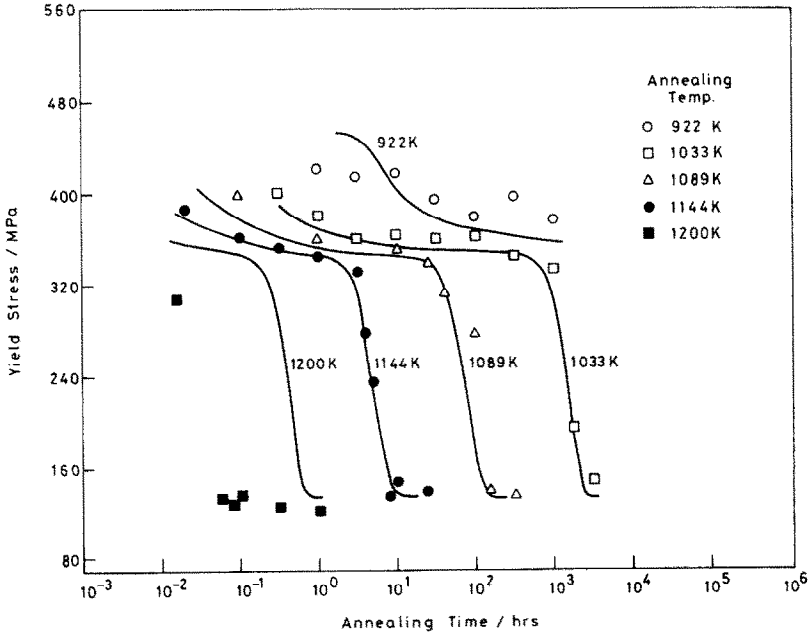

Fig. 2. Yield stress of 20% cold-worked AISI 316 steel measured at 811 K following high temperature annealing, compared with calculation (solid lines).

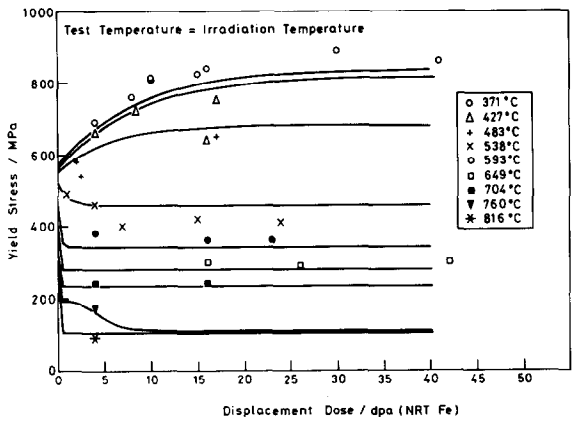

Fig. 3. Evolution of yield stress of 20% cold-worked AISI 316 steel with irradiation damage dose at various temperatures.

$3.7 \times 10^{-5} \exp(-33615/T)$ m^2 s^{-1} [12] and $\alpha_0 = 0.0654$. The effect of irradiation at various temperatures is shown in fig. 3, which determines the remaining constants. The low temperature data provide values for a and c and the behaviour at higher temperatures gives additional checks on b and α_0. The apparent saturation of the yield stress with increasing dose corresponds to the steady state result:

$$\alpha = \alpha_0 + \left(\frac{a\dot{D}}{bD_s + c\dot{D}} \right)^{1/2}. \tag{6}$$

The calculations shown in fig. 3 use $a = 0.03$ dpa (NRT Fe)$^{-1}$, $b = 1.2 \times 10^{17}$ m^{-2}, $c = 0.15$ dpa (NRT Fe)$^{-1}$ with α initially equal to 0.2. A dose rate of 0.87 dpa (NRT Fe)/s has been used to represent the EBR-II irradiation.

The models described so far are improvements on empirical correlations devised to fit the data shown in fig. 3. The hardness evolution equation and recrystallisation equation are dynamical equations which can treat changing conditions, not just the steady state conditions of the experiments, and since the form of the equations is based on mechanistic considerations, a departure from the steady state can be made with some degree of confidence. In this respect our approach is similar to that of DiMelfi and Kramer [13] though we base our modelling on eq. (1) rather than the Voce correlation.

3. The constitutive relation

The relationship between stress and strain is an important aspect of transgranular failure by plastic yield deformation. An important feature of dislocation dynamics is the generation of new dislocations during motion. Using the Orowan relation for the plastic strain rate $\dot{\epsilon}$ and a suitable multiplication equation for ρ we have

$$\begin{aligned} \dot{\epsilon} &= b\rho v, \\ \dot{\rho} &= R\rho, \end{aligned} \tag{7}$$

where b is the Burger's vector, v the dislocation velocity and R a multiplication rate associated with the density of the dislocation sources. Assuming the dislocation velocity is a constant during deformation this yields the relation $\dot{\rho} \propto \dot{\epsilon}$: this is the basis of the assertion in the previous section that the initial dislocation density is proportional to the cold work strain. We therefore have an additional term in the evolution equation for α corresponding to the effects of plastic strain:

$$\dot{\alpha} = \dot{\epsilon} + \text{previous terms}. \tag{8}$$

Neglecting any contribution to $\dot{\alpha}$ from the previous terms (in eq. (3)) during a rapid deformation, this yields a parabolic constitutive relation between σ_y and ϵ:

$$\sigma_y = \sigma_0 + A\left((1 - f_R)(\epsilon + \epsilon_0)\right)^{1/2}, \tag{9}$$

where ϵ_0 is the value of α prior to the deformation. Clearly, the constitutive relation is a function of the previous history of the material, represented by ϵ_0, and also depends on current temperature conditions, embodied in the T-dependence of σ_0 and A. The work hardening coefficient $d\sigma_y/d\epsilon$ is characteristic of the deformation and failure behaviour and is lower following irradiation below about 500 °C than in the fresh state (corresponding to an increase in ϵ_0). This corresponds to an increased tendency to suffer large strains following initial yield but also increases the likelihood of instability during yield, and loss of ductility, which we shall examine later.

The form of eq. (9) is confirmed by data shown in fig. 4: a history dependent shift of stress-strain data [14] along the strain axis, by a value ϵ_0 calculated using the previously described evolution model, brings about a coalescence of the results of several tensile tests onto the same line.

4. Fracture

The intervention of fracture during the process of yield deformation is a far more difficult phenomenon to model than the evolution of the yield stress. Fracture involves the local influence of inhomogeneities in concentrating stress and initiating the tearing of the

material. Our task, then, is to represent the effects of inhomogeneities in a homogeneous fashion, i.e. as a single macroscopic constitutive relation. A complete microscopic description of this would be too complicated for our requirements and it may be necessary to impose a limiting ductility on the deformation. However, the potential for unstable yield deformation is reflected in the form of the constitutive relation, eq. (9) and trends in the fracture behaviour of irradiated cladding can be described.

An analysis of instability during yield has been presented for a number of simple constitutive relations which illustrate this point [15]. For a yield law $\epsilon \propto \sigma^{1/m}$ it can be shown that a uniform specimen meets an instability in deformation at a failure strain $\epsilon_f = m$, and that cold work and solute hardening reduce this ductility. In addition, ϵ_f is sensitive to slight geometric defects in the specimen: if this is represented by a local thinning of a tensile specimen by a relative factor $(1-\delta)$ then for the above constitutive relation ϵ_f is given by:

$$m^m \exp(-m)(1-\delta) = \epsilon_f^m \exp(-\epsilon_f), \qquad (10)$$

which gives $d\epsilon_f/d\delta \to -\infty$ in the limit $\delta \to 0$, i.e. strong sensitivity of ductility to geometric defects. This is illustrated in fig. 5.

We shall not consider local geometric defects here, though they clearly can have a strong effect on the onset of fracture. We shall concentrate on instabilities in the flow in a uniform specimen. This is characterised by the following condition, for a uniaxial tensile test:

$$\frac{1}{\sigma}\frac{d\sigma}{d\epsilon} = 1, \qquad (11)$$

which is a generalisation of the result given above for the $\epsilon \propto \sigma^{1/m}$ constitutive relation. The instability corresponds to the inability of work hardening to keep up with the stress enhancement due to specimen thinning during deformaton.

The remainder of this paper examines the potential for instability in the constitutive relation introduced by considering the effects of pores in the cladding. This defect is given special consideration since cladding exposed to a fast neutron flux suffers a swelling due to the formation of voids, driven by vacancy production due to displacement damage. The porosity can become very high over a long irradiation. What is more, loss of ductility has been correlated experimentally with the swelling suffered by the clad [16,17]. The most highly swollen specimens exhibited the most brittle tensile properties.

Porosity alters the yield behaviour of a material in two ways. The yield stress is reduced as a result of stress concentration between the pores, and the rate of work hardening is reduced as a result of additional strain arising from the dilation of the pores. These alterations are described by equations due to Gurson [18], with

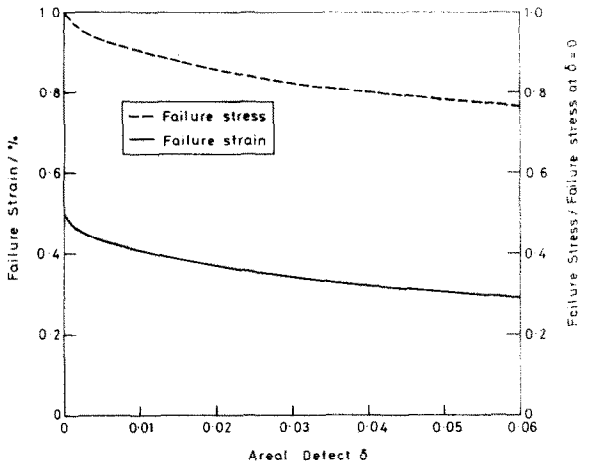

Fig. 5. Effect of local areal defect δ on failure strain δ_f and ultimate tensile stress σ_{UTS}.

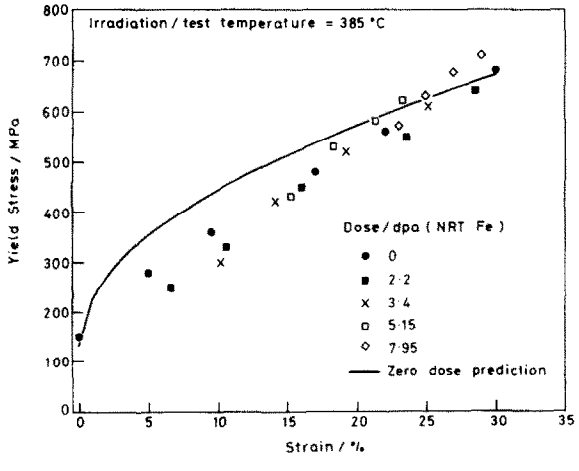

Fig. 4. Stress–strain data [14], adjusted by shifts of strain origin for various irradiated samples of annealed AISI 316 steel.

subsequent modification by Tvergaard [19]. The yield strain rate tensor is given by

$$\dot{\epsilon}^{\mathrm{p}}_{ij} = \dot{\lambda}\frac{\partial \phi}{\partial \sigma_{ij}}, \tag{12}$$

where σ_{ij} is the macroscopic stress tensor and

$$\phi = \frac{\sigma_e^2}{\sigma_y^2} + 2q_1 f^* \cosh\frac{q_2\sigma_{kk}}{2\sigma_y} - 1 - q_1^2 f^{*2}, \tag{13}$$

with σ_e the von Mises' stress given by $(\frac{3}{2}s_{ij}s_{ij})^{1/2}$ (summation over repeated indices) where $s_{ij} = \sigma_{ij} - \frac{1}{3}\delta_{ij}\sigma_{kk}$. The local yield stress of the matrix material between the voids is represented by σ_y. f^* is a function of the fractional porosity f and is given here by

$$\begin{aligned} f^* &= f; \quad f < f_c = 0.15, \\ &= f + \left(\frac{f - f_c}{f_F - f_c}\right)^2 (f_u - f_F); \quad f > f_c = 0.15, \\ & \qquad f < f_F = 0.25, \end{aligned} \tag{14}$$

where $f_u = 1/q_1$. The behaviour for $f > 0.15$ is meant to represent the coalescence of pores. The parameters q_1 and q_2 are equal to 1.5 and 1.0, respectively. A similar formalism has been used with some success in describing the failure of porous substances (failure is indicated by the condition $f^* = f_u$, when the macroscopic yield stress vanishes). The flow rate parameter $\dot{\lambda}$ can be expressed in terms of known quantities, and the evolution of f is described by a combination of pore growth and nucleation, the latter controlled by stress or strain criteria [20,21].

The plastic potential ϕ represents the yield condition and the constitutive relation. There is no yield for $\phi < 0$ and during yield $\phi = 0$. It is helpful to consider the formalism for the non-porous case: $f = 0$. Yield occurs in this case when $\sigma_e = \sigma_y$ and the constitutive relation is

$$\dot{\epsilon}^{\mathrm{p}}_{ij} = \frac{3\dot{\lambda}s_{ij}}{\sigma_y^2}, \tag{15}$$

which is the Prandtl–Reuss equation. Eq. (13) describes modifications to this basic behaviour for a porous material. Macroscopically, the deformation is not volume conserving when there is porosity. The porosity evolves according to

$$\dot{f} = (1 - f)\dot{\epsilon}^{\mathrm{p}}_{ii} + \dot{S}, \tag{16}$$

where $\dot{S}$ is the void swelling rate.

The deformation equations can be applied to the case of a tensile test under a uniaxial stress σ [22]. The evolution of the various parameters is given by

$$\begin{aligned} \dot{\epsilon}^{\mathrm{p}} &= \frac{\sigma_y^2}{\sigma^2} G'(1 - f)\dot{L}, \\ \dot{\sigma}_y &= \frac{\sigma_y}{\sigma}\dot{L}, \\ \dot{f} &= \frac{(1 - f)^2 g\sigma_y^2 G'}{\sigma^2\left(2\sigma/\sigma_y^2 + g/3\right)}\dot{L}, \\ \dot{L} &= \frac{\dot{\sigma}}{1 - \gamma f^{*\prime}(1 - f)g}; \end{aligned} \tag{17}$$

where ϵ^{p} is the uniaxial plastic strain and

$$\begin{aligned} \gamma &= 2q_1\left(\cosh\frac{q_2\sigma}{2\sigma_y} - q_1 f^*\right)\frac{\sigma_y^2 G'(1 - f)}{\sigma^2\left(2\sigma/\sigma_y^2 + g/3\right)^2}, \\ g &= \frac{3q_1q_2}{\sigma_y} f^* \sinh\frac{q_2\sigma}{2\sigma_y}, \end{aligned} \tag{18}$$

and $f^{*\prime}$ is $\mathrm{d}f^*/\mathrm{d}f$, G' is $\mathrm{d}G/\mathrm{d}\sigma_y$ and $\epsilon^{\mathrm{p}} = G(\sigma)$ is the uniaxial stress–strain relation for the matrix material. Note that the usual deformation equations are obtained in the limit $f \to 0$ ($\sigma_y = \sigma$, $\dot{\epsilon}^{\mathrm{p}} = G'\dot{\sigma}$). The series of equations may appear complex, but basically they just represent the two effects alluded to earlier: the reduction in the macroscopic yield stress and the decrease in the work hardening rate. This second aspect is illustrated by the form for $\dot{L}$: the factor $(1 - \gamma f^{*\prime}(1 - f)g)$ in the denominator accelerates the evolution of plastic strain, for a given rate of increase in stress $\dot{\sigma}$, as porosity develops. The condition of plastic instability (eq. 11) is now replaced by

$$\frac{1}{\sigma}\frac{\mathrm{d}\sigma}{\mathrm{d}\epsilon^{\mathrm{p}}} \le 1 - \frac{g}{2\sigma/\sigma_y^2 + g/3}, \tag{19}$$

which differs only slightly from the non-porous case.

We have tested the model by calculating the deformation, in uniaxial tensile tests at room temperature (293 K), of specimens of irradiated 20% AISI 316 cladding. We take as input the observed yield stress and the swelling porosity and use eq. (9) as the basic constitutive relation in eqs. (17). The deformation is calculated until the instability is met. We have used swelling data from Dupouy et al. [16], reproduced in fig. 6, where we also show the observed ultimate tensile strengths. The room temperature data are provided by Dupouy et al. as a function of position along the pin. Unfortunately, clear details of irradiation temperatures as a function of position were not given. However, we can make estimates from the information provided, and

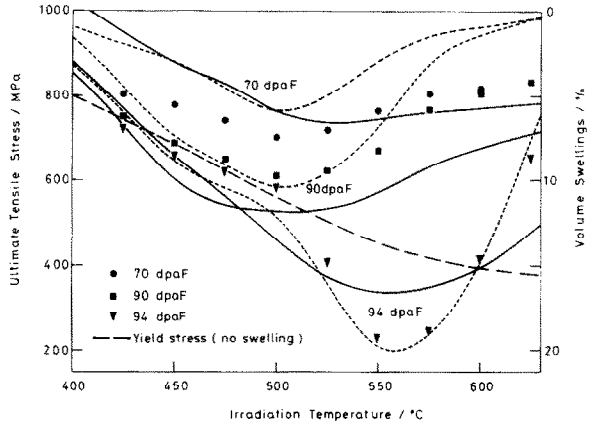

Fig. 6. Room temperature ultimate tensile stresses (solid lines) and swellings (dotted lines) at doses shown against irradiation temperature (from Dupouy et al. [16]). Points are calculated ultimate tensile stresses.

then use the data from ref. [5] indicating the room temperature yield stress of the cladding as a function of the irradiation temperature. Both sets of data are from Phenix irradiations. Errors arising from this procedure should not alter the results of our calculations qualitatively. The deduced yield stresses are also shown in fig. 6. We assume that these values refer to non-porous (or at least only slightly porous) material and so interpret them as initial values of σ_y. The actual yield stress of the swollen cladding is then a function of the porosity, using the earlier equation for $\phi = 0$.

The calculated ultimate tensile stresses (UTS) are shown in fig. 6 and the associated uniform elongations in fig. 7, where a comparison is made with the actual ductilities [16]. There is a clear correlation between high swelling and low UTS which our model can account for. This is accompanied by a loss of ductility, with total brittleness occurring for a swelling of about 20%, in agreement with the data. The failure strains are generally too high (though showing the correct qualitative trends) and may indicate a local rather than a uniform strain. Indeed the model assumes a spatially uniform porosity in the material, discounting the possibility of fluctuations, which have an important bearing on the yield behaviour. However, the important conclusion is that the correlation of high swelling with poor mechanical properties can be explained, and consideration of local defects will have to be left for future development.

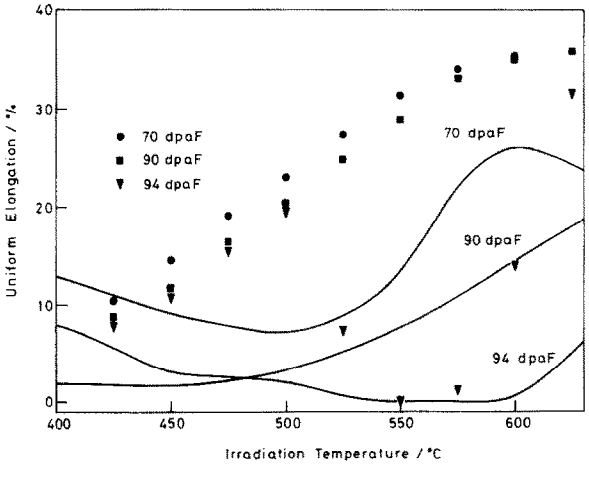

Fig. 7. Room temperature uniform elongations (solid lines) against irradiation temperature, for doses shown (from Dupouy et al. [16]). Points are sample calculations.

5. Conclusions

The mechanical fracture of Fast Reactor cladding has been considered using mechanistic theories in order to improve our modelling of fuel pin failure in possible accidents. The mechanisms which produce intergranular fracture are dealt with elsewhere [23]: here we have considered the transgranular mode of failure which operates at low temperatures and gives rise to fast fractures.

Our modelling has concentrated on two aspects: the constitutive relation for deformation and the yield stress. A model has been developed, based on dislocation theory, which compares well against the changes in yield stress induced by high temperatures and neutron irradiation. We have found, however, that a homogeneous constitutive relation alone cannot fully represent the occurrence of fracture since yield deformation is sensitive to small defects in the geometry of the specimen. It is able to reflect trends in the onset of failure, however, which we have illustrated by considering the change in failure characteristics induced by neutron-induced swelling porosity. Large reductions in ductility are associated with high swelling fractions, with complete brittleness in 20% cold-worked AISI 316 stainless steel appearing at a swelling of about 20%. The calculations, however, overestimate the failure strains and could be interpreted as local strains.

The modelling of transgranular failure on a level which ignores specimen defects must then necessarily introduce an artificial failure criterion such as a preset failure strain. Our experience with modelling the deformation of Fast Reactor fuel pins using eq. (9) in the TRAFIC code has suggested that this is a reasonably

fruitful approach. The changes in the constitutive relation due to evolution of α in eq. (3), coupled with the cylindrical geometry of the cladding tube, with its potential for instability, produce a yield behaviour which is relatively unstable beyond an effective plastic strain of 1–2% and a preset limit of 3% has produced good agreement with experimental failure times [24].

In conclusion, we have shown that simple physical considerations can provide models which describe the very complicated processes of yield deformation in Fast Reactor irradiated fuel pin cladding. Although the fracture process is not itself described microscopically, the models can help in identifying the onset of failure, by the occurrence of a plastic instability. A more general analysis including local effects is left to the future.

Acknowledgements

This work has been supported in part by the Corporate Research Programme of AEA Technology, and in part by the Commission of the European Communities, Joint Research Centre, Ispra Establishment. The author thanks Dr. J.R. Matthews for useful discussions.

References

[1] J.R. Matthews, R.F. Cameron, P.E. Coleman and R. Thetford, The application of the TRAFIC code to Fast Reactor fuel transients, presented at BNES Conf. on Fast Reactor safety, Guernsey, May 1986.
[2] K. Lassmann and H. Blank, Nucl. Eng. Des. 106 (1988) 291.
[3] G.I. Taylor, Proc. Roy. Soc. London A145 (1934) 362.
[4] R.L. Fish and J.J. Holmes, J. Nucl. Mater. 46 (1973) 113.
[5] M. Balourdet and R. Cauvin, Transient mechanical properties of CABRI-1 cladding (cw 316), presented at BNES Conf. on Fast Reactor Core and Fuel Structure Behaviour, Inverness, June 1990.
[6] R.L. Fish, N.S. Cannon and G.L. Wire, in: Proc. Conf. on Effects of Radiation on Structural Materials, ASTM-STP 683, Eds. J.A. Sprague and D. Kramer (American Society for Testing and Materials, Philadelphia 1979) p. 450.
[7] P. Gay, P.B. Hirsch and A. Kelly, Acta Crystallogr. 7 (1954) 41.
[8] J.R. Matthews, A Simple Dislocation Model for High-Temperature Deformation, Harwell report AERE-R11564 (1985).
[9] J.R. Matthews, private communication.
[10] A.G. Guy, Introduction to Materials Science (McGraw–Hill, New York, 1972) p. 375.
[11] M.M. Paxton and J.J. Holmes, Hanford Engineering Development Laboratory report HEDL-TME-71-126 (1971).
[12] R.A. Perkins, R.A. Padgett and N.K. Tanali, Metall. Trans. 4 (1973) 2535.
[13] R.J. DiMelfi and J.M. Kramer, J. Nucl. Mater. 89 (1980) 338.
[14] A.L. Ward and L.D. Blackburn, Hanford Engineering Development Laboratory report HEDL-TME-78-51 (1978).
[15] J.R. Matthews, An Introduction to Thermomechanics (Including Radiation Effects), Harwell report AERE-R13450 (1989).
[16] J.M. Dupouy, J.P. Sagot and J.L. Boutard, presented at BNES Conf. on Dimensional Stability and Mechanical Behaviour of Irradiated Metals and Alloys, Brighton, 1983.
[17] V. Levy, J.L. Seran, A. Maillard, T. Martella, H.J. Bergmann, W. Dietz, K. Ehrlich, K. Herschbach, M. Lippens and Y. Vanderborck, Cold worked 15Cr15NiTi-MoB alloys for cladding application in Fast Breeder reactors, in: Proc BNES Conf. on Fast Reactor core and fuel structural behaviour, Inverness, June 1990, paper 46.
[18] A.L. Gurson, J. Eng. Mater. Technol. 99 (1977) 2.
[19] V. Tvergaard, Int. J. Fracture 17 (1981) 389; 18 (1982) 237.
[20] A. Needleman and J.R. Rice, in: Mechanics of Sheet Metal Forming, Eds. D.P. Koistinen et al. (Plenum, New York, 1978) p. 237.
[21] M.Saje, J. Pan and A. Needleman, Int. Fracture 19 (1982) 163.
[22] I.J. Ford and J.R. Matthews, Constitutive relations for deformation and failure of Fast Reactor cladding tubes, in: Proc. 19th Canadian Fracture Conference, Ottawa, 1989, Eds. A.S. Krausz, J.I. Dickson, J.P.A. Immarigeon and W. Wallace (Kluwer Academic Publishers, 1990).
[23] I.J. Ford, Intergranular Fracture of Fast Reactor Irradiated Stainless Steel, Harwell Report TP.1347 (1990).
[24] I.J. Ford, R. Thetford, P. Edwards and N.P. Taylor, Mechanistic models of clad failure and molten fuel behaviour in the TRAFIC2 code and their application to transients, in: Proc. Int. Fast Reactor Safety Meeting, Snowbird, Utah, August 1990.